Supplementary Table 1. Expression pattern of MKL1/MKL2/SRF downstream genes in BXD2 mice post-LTβR-Fc administration or are deficient of type I IFNAR

Symbol	Targeted Effects by MKL1/2/SRF	LTR-Fc vs. Vehicle	*Ifnar-/-* vs. *Ifnar+/+*	Gene Type(s)	Coding Protein
IL4	Inhibit	2.616	1.949	cytokine	Interleukin 4
CYBA	Inhibit	2.071	2.282	enzyme	Cytochrome B-245, Alpha Polypeptide
EPX	Inhibit	7.301	-1.107	enzyme	Eosinophil peroxidase
GSTM5	Inhibit	3.447	-1.165	enzyme	Glutathione S-transferase mu 5
CDKN1A	Inhibit	2.501	1.41	kinase	cyclin-dependent kinase inhibitor 1A
CLDN15	Inhibit	3.851	-1.546	other	Claudin 15
Dmkn	Inhibit	2.127	-1.101	other	Dermokine
DNAJB4	Inhibit	2.876	1.308	other	DnaJ (Hsp40) homolog, subfamily B, member 4
DSTN	Inhibit	2.092	-1.21	other	Destrin (actin depolymerizing factor)
FCN1	Inhibit	3.347	-1.112	other	Ficolin (collagen/fibrinogen domain containing) 1
IER2	Inhibit	5.059	1.267	other	immediate early response 2
MS4A3	Inhibit	3.886	-1.917	other	Membrane-spanning 4-domains, subfamily A, member 3 (hematopoietic cell-specific)
PRG2	Inhibit	4.664	-1.335	other	Proteoglycan 2, bone marrow (natural killer cell activator, eosinophil granule major basic protein)
PRG3	Inhibit	6.03	-1.065	other	Proteoglycan 3
SLPI	Inhibit	2.649	-1.374	other	Secretory leukocyte peptidase inhibitor
CPA3	Inhibit	4.017	-1.053	peptidase	Carboxypeptidase A3 (mast cell)
CTSG	Inhibit	2.602	-2.806	peptidase	Cathepsin G
ELANE	Inhibit	5.809	-1.817	peptidase	Elastase, neutrophil expressed
Mcpt8	Inhibit	2.039	-3.154	peptidase	Mast cell protease 8
Prss34	Inhibit	3.552	-2.848	peptidase	Protease, serine 34
PRTN3	Inhibit	3.695	-2.243	peptidase	Proteinase 3
CEBPE	Inhibit	3.351	-1.178	transcription regulator	CCAAT/enhancer binding protein (C/EBP), epsilon
EGR1	Inhibit	3.02	1.507	transcription regulator	Early growth response 1
ETS1	Enhance	-2.066	-1.096	transcription regulator	v-ets avian erythroblastosis virus E26 oncogene homolog 1
FOS	Inhibit	2.791	2.236	transcription regulator	FBJ murine osteosarcoma viral oncogene homolog
FOSB	Inhibit	6.372	3.19	transcription regulator	FBJ murine osteosarcoma viral oncogene homolog B
GFI1	Inhibit	2.007	-1.239	transcription regulator	Growth factor independent 1 transcription repressor
JUN	Inhibit	3.46	1.658	transcription regulator	Jun proto-oncogene
JUNB	Inhibit	4.532	3.13	transcription regulator	Jun B proto-oncogene
IFITM1	Inhibit	3.369	2.255	transmembrane receptor	Interferon induced transmembrane protein 1
RAMP1	Inhibit	3.176	1.467	transporter	Receptor (G protein-coupled) activity modifying protein 1

Upregulated — Downregulated

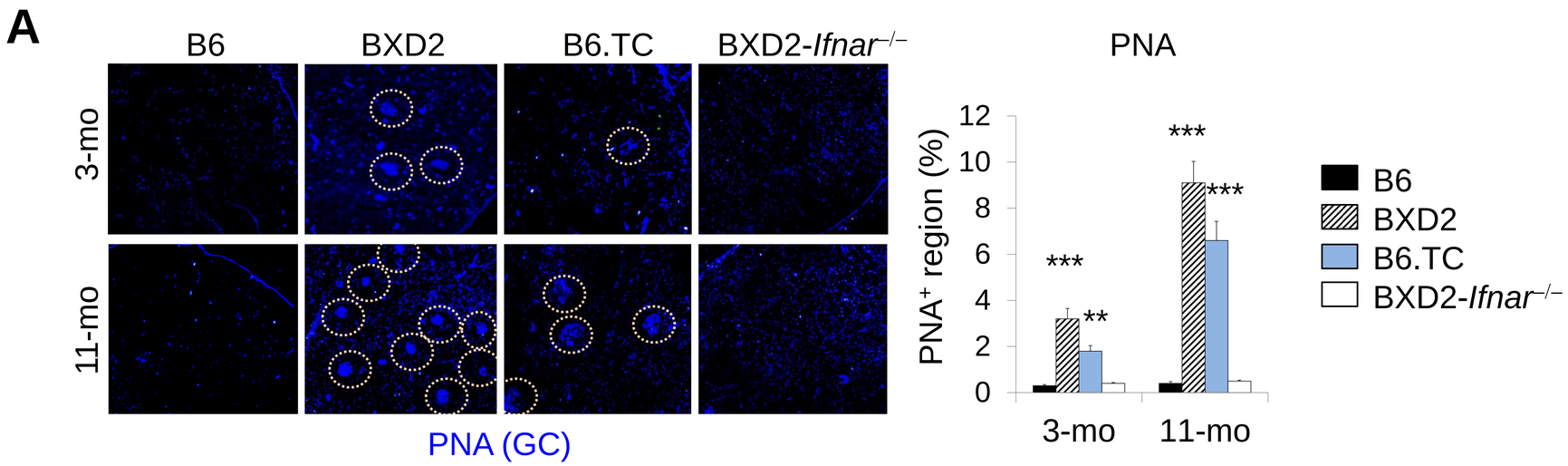

Supplemental Figure 1. Age-related development of spontaneous germinal centers and circulating autoantibodies in BXD2 and B6.TC mice.

(**A**) Spleens obtained from B6, BXD2, B6.TC, and BXD2-*Ifnar*$^{-/-}$ mice at 3-mo-old and 11-mo-old were analyzed by confocal imaging microscopy. Representative fluorescent photomicrographs of PNA^{+} GCs (circled blue) (Objective lens, 4x) are shown in the left, and quantitation of the percent of PNA^{+} area per microscopic region is shown in the right. All images are representative spleen regions. (**B**) ELISA analysis of the indicated IgG autoantibody titers in sera obtained from 3- or 11-mo-old mice of the indicated strains. All data are mean ± SEM. (*P < 0.05, **P < 0.01, ***P < 0.005 vs control or B6. n = 2-3 mice per group for 2 independent experiments, Student's test).

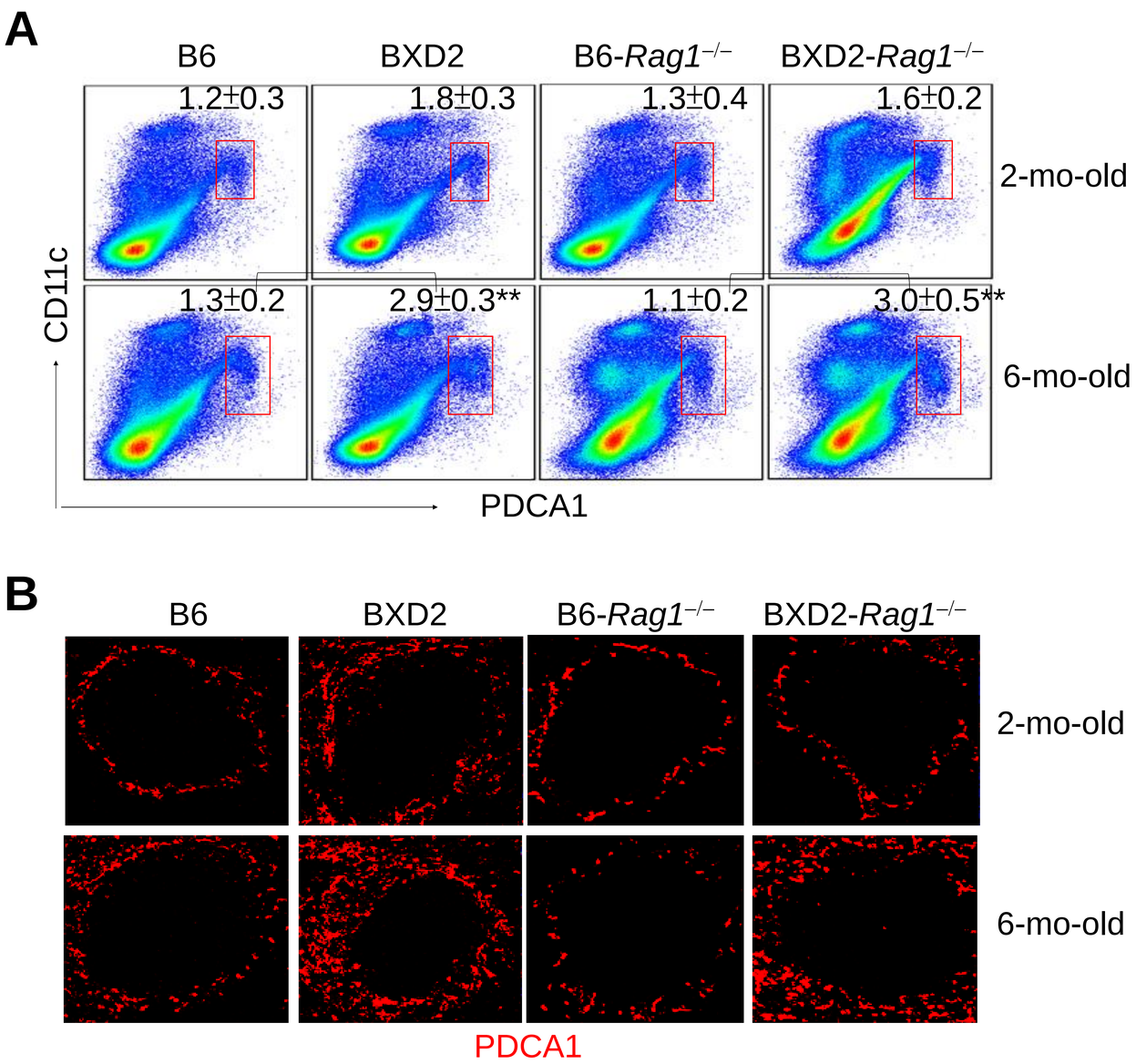

Supplemental Figure 2. Comparable numbers and localization of pDCs in the spleen of WT and *Rag1*$^{-/-}$ mice.
(**A**) FACS analysis of the percent of PDCA1^{+}CD11c^{Int} pDCs in the spleens of the indicated strains of mice at 2-mo-old (top panels) or 6-mo-old (bottom panels). (**B**) Confocal microscopic imaging analysis of PDCA1 expression in the indicated strains of mouse spleen at either 2-mo-old (top panels) or 6-mo-old (bottom panels). Images shown are derived from a representative spleen follicle from each group. (**C**) Quantitative qRT-PCR analysis of the expression of genes encoding the indicated type I IFNs in PBMCs in 6-mo-old mice. All data are mean ± SEM (*n* = 2-3 per group for 2 independent experiments; **P* < 0.05, ***P* < 0.01, ****P* < 0.005 between the indicated comparisons, Student's t-test).

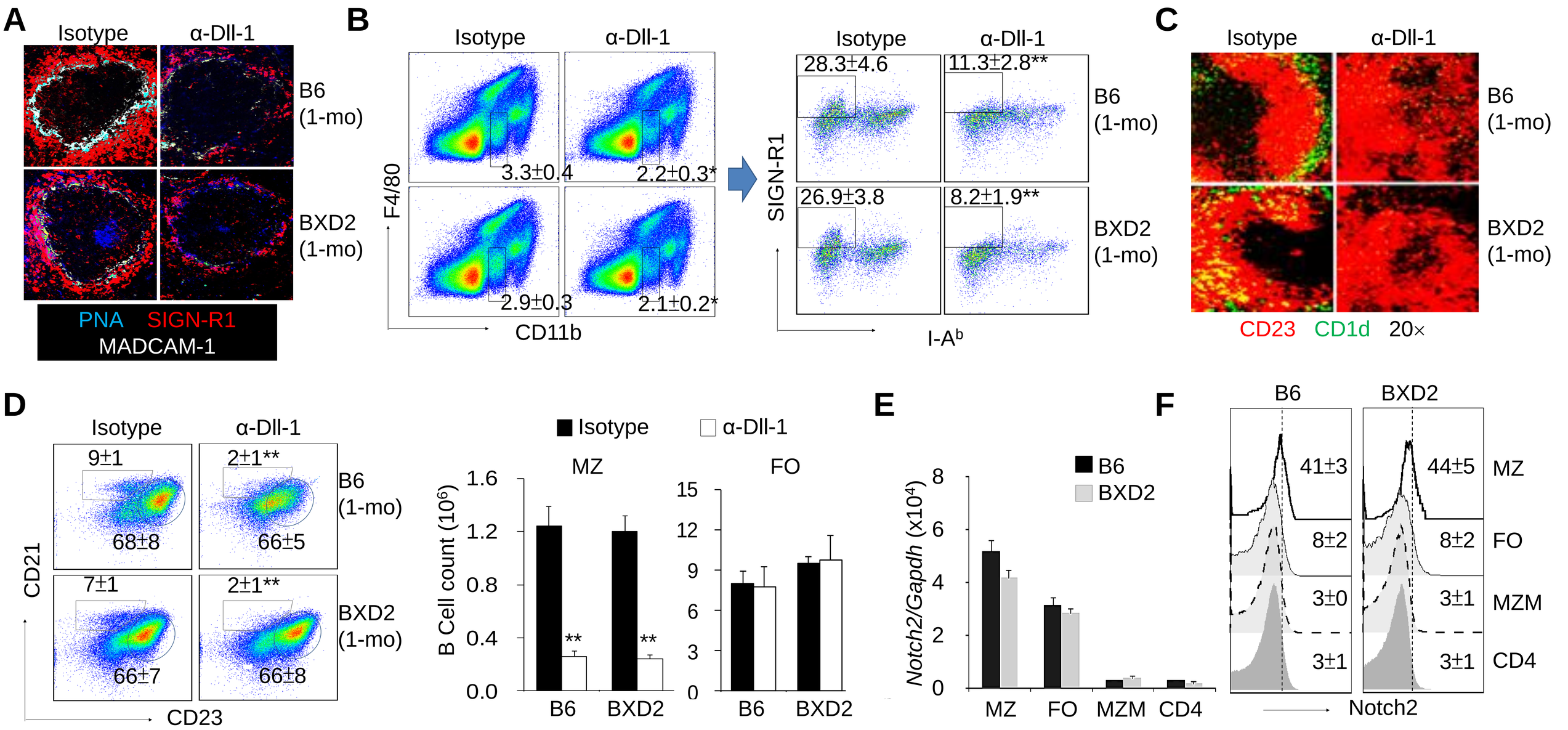

Supplemental Figure 3. Depletion of Notch2^{+} MZ B cells resulted in reduction of MZMs.
(**A-D**) B6 and BXD2 mice (both 1-mo-old) were treated with either an isotype control or an anti-Dll-1 antibody (200 μg/mouse, 1x per wk for 1 month). (**A**) Confocal microscopic imaging analysis of PNA^{+} GC B cells, SIGN-R1^{+} MZMs and MADCAM-1^{+} endothelial cells in the spleen. A representative image from each group is shown. (**B**) Flow cytometry analysis showing the frequency of CD11b^{lo}F4/80^{neg}SIGN-R1^{+}I-A^{b-} MZMs (rectangle) gated cells in the spleen, (**C**) Confocal microscopic imaging analysis of CD1d^{+} MZ B cells and CD23^{+} B cells in the spleen. A representative image from each group is shown. (**D**) FACS analysis of the percent (left) and total cell count (right) of MZ (CD21^{hi}CD23^{lo}, boxed in upper left) or FO (CD21^{lo}CD23^{hi}, circled in lower right) in CD19^{+} gated B cells. (**E**) qRT-PCR analysis of *Notch2* expression in FACS sorted MZ (IgM^{hi}CD21^{hi}CD23^{lo}) CD19^{+} B cells, FO (IgM^{lo}CD21^{lo}CD23^{hi}) CD19^{+} B cells, MZMs (CD11b^{lo}F4/80^{neg}SIGN-R1^{+}I-A^{b-}) and CD4 T cells from the spleen of naïve B6 and BXD2 mice. (**F**) Flow cytometry analysis of Notch2 expression on the surface of MZ, FO, MZM, and CD4 T cells in B6 and BXD2 mice. All data are mean ± SEM (*n* = 3 per group for 2 independent experiments. *P < 0.05 and **P < 0.01 between results from isotype treated B6 or BXD2 mice versus anti-Dll-1 treated B6 or BXD2 mice, Student's t-test).

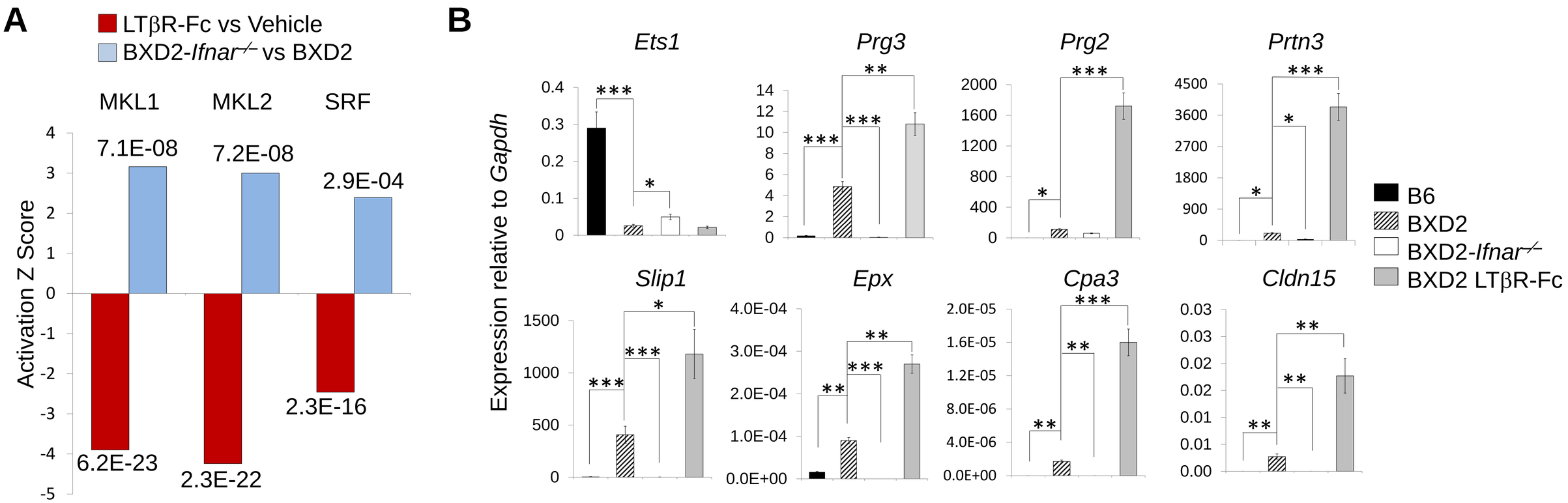

Supplemental Figure 4. Alteration of the MKL1/MKL2/SRF pathway in BXD2 mice that were treated with LTβR-Fc or are deficient of IFNAR.

MZMs were sorted by flow cytometry from the spleens of 2.5-mo-old BXD2 mice that were treated with PBS or LTβR-Fc (injected i.v. with 25 μg sLTβR-Fc), and BXD2-*Ifnar*$^{-/-}$ mice treated with PBS. Mice were sacrificed 10 hrs following the treatment. RNA was isolated via a TRIzol method (Invitrogen). (**A**) Gene array upstream pathway analysis of genes regulated by MKL1, MKL2 and SRF in sorted MZMs from vehicle- vs LTβR-Fc-administered BXD2 mice or BXD2-*Ifnar*$^{+/+}$ vs. BXD2-*Ifnar*$^{-/-}$ mice. Gene expression analysis was performed using the mouse WG-6 BeadChip and iScan system from Illumina, Inc. Total RNA was converted to cDNA by reverse transcription, followed by second-strand synthesis to generate double-stranded cDNA. After purification, the cDNA was converted to biotin-labeled cRNA, hybridized to a mouse WG-6 BeadChip and stained with strepavidin-Cy3 for visualization. The mouse WG-6 BeadChips contain sequences representing approximately 45,200 curated and putative genes and ESTs. Quality standards for hybridization, labeling, staining, background signal, and basal level of housekeeping gene expression for each chip were verified. After scanning the probe array, the resulting image was analyzed using GenomeStudio software (v2011.1, Illumina, Inc.). Gene lists were further analyzed using GeneSpring version 12.1 (Agilent) software. Data were analyzed through the use of Ingenuity Pathways Analysis (IPA, Ingenuity® Systems, www.ingenuity.com). Upstream Regulator Analysis from IPA was used to identify the upstream regulators that were responsible for gene expression changes observed in the data. The activation z-score (an algorithm designed to reduce the chance that random data will generate significant predictions) identifies upstream regulators that can explain observed gene expression changes in the data, and predicts the activation state of the upstream regulators. An absolute z-score ≥ 2 is considered significant. Predictions where both the z-score is significant (absolute value ≥ 2) and the p-value is significant (<10^{E-3}) are the most reliable predictions. The results were obtained from a pool of 2 mouse spleens per chip from each group for 2 chips from BXD2 mice and 1 chip from the other 2 groups). The P value for each comparison is shown. (**B**) qRT-PCR analysis of representative genes that are regulated by the MKL-SRF axis in sorted MZMs from the indicated strains. All data are mean ± SEM from each group (*P < 0.05, **P < 0.01, ***P < 0.005 between the indicated groups. n = 2-3 mice per group for 2 independent experiments, Student's t-test). The full name of each gene is shown in Supplementary Table 1.

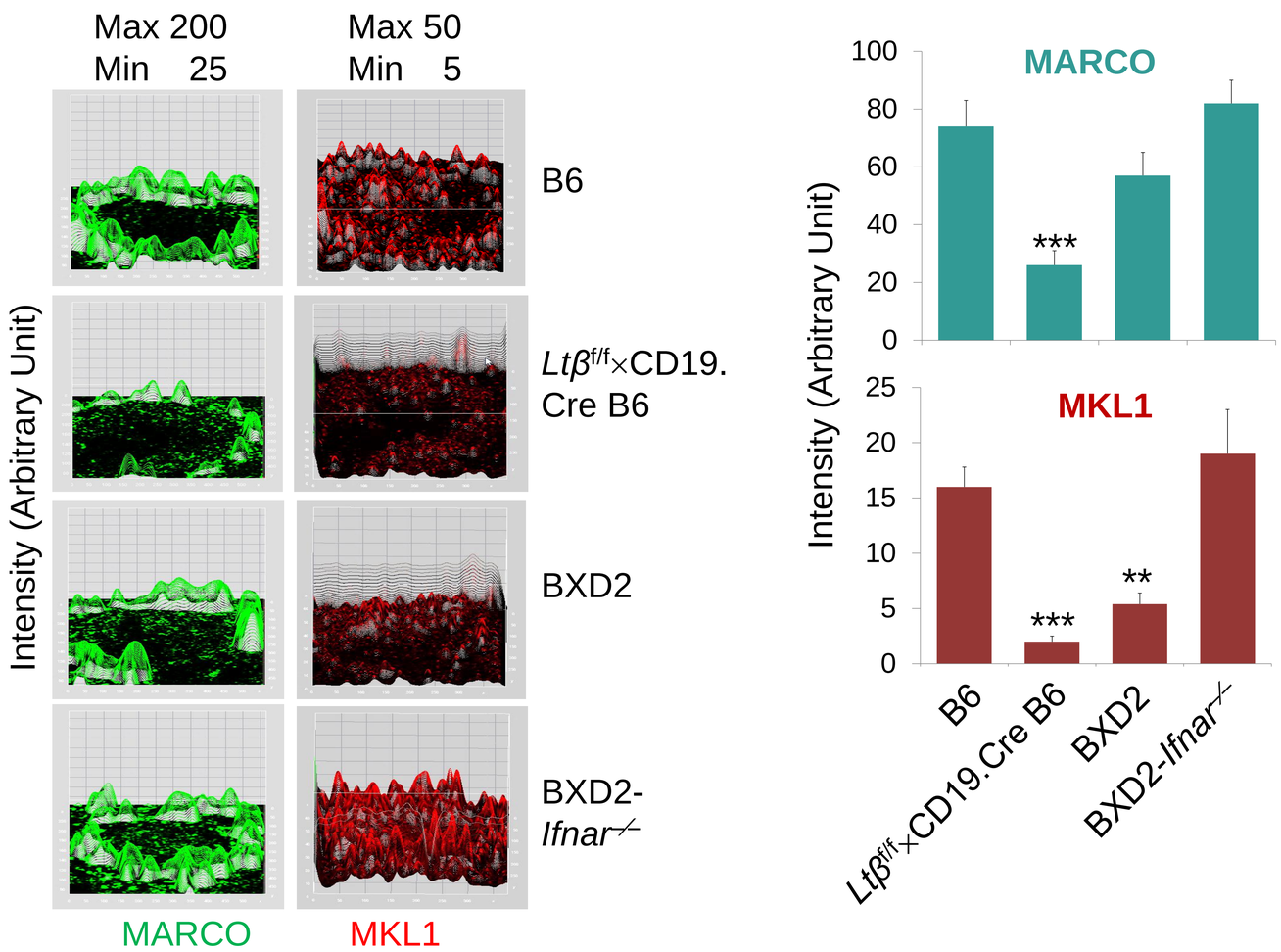

Supplemental Figure 5. Defective LTβR signaling or increased IFNAR signaling is associated with decreased expression of MKL1 in MZMs. Right: Representative ImageJ 3D intensity plots of MARCO (green) or MKL1 (red) in the indicated mouse spleen follicle. Original images were acquired using confocal imaging microscopy (objective lens 20×). The maximal and minimal intensity scales set for the plots are shown on the top. left: ImageJ quantitation of the intensity of either MARCO or MKL1. Results are the average from 3–5 randomly chosen follicles analyzed per section (***P* < 0.01 or ** *P* < 0,005 versus B6. n = 2-3 mice per group for 2 independent experiments, Student's t-test).

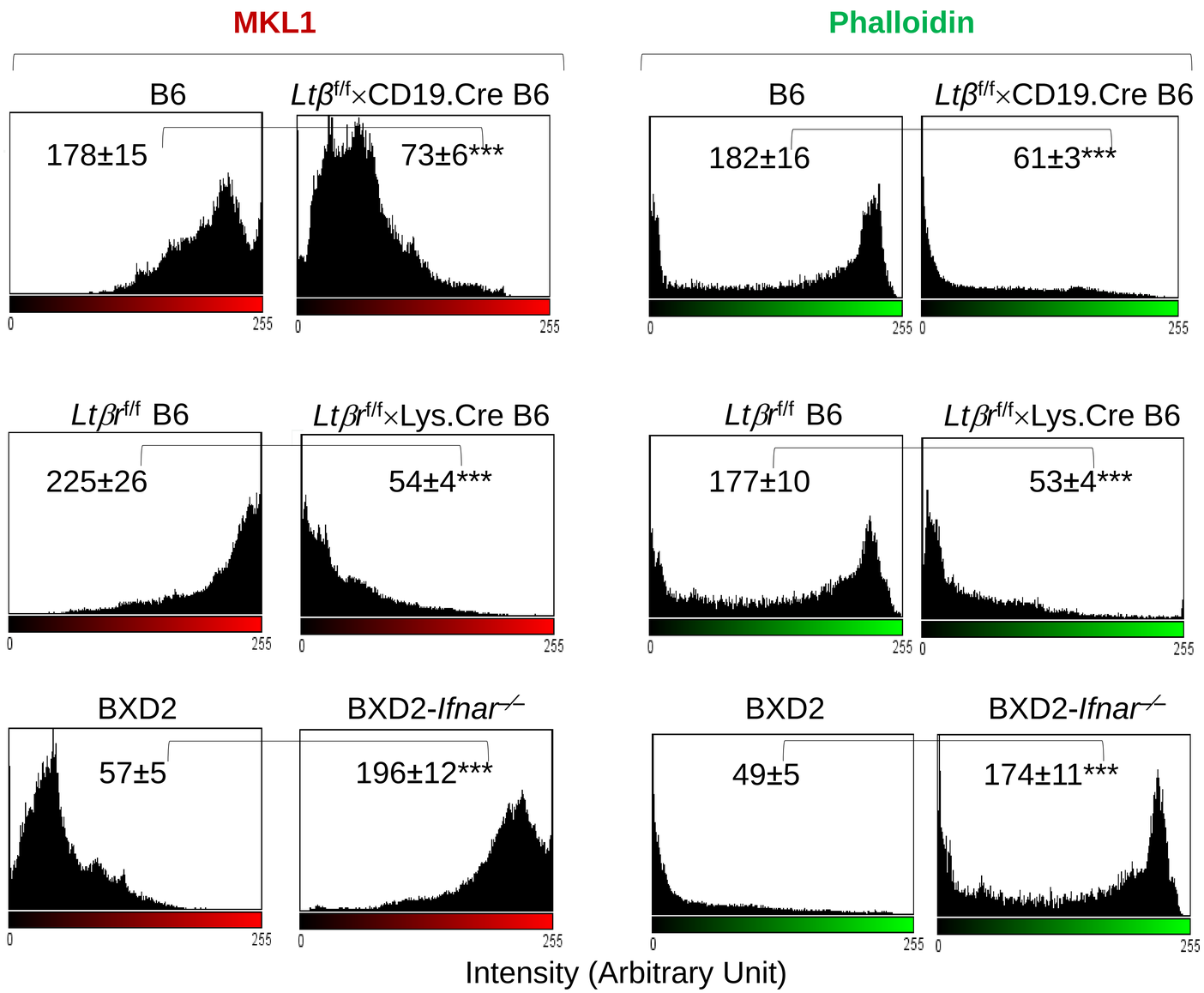

Supplemental Figure 6. Defective LTβR signaling is associated with decreased mechanosensing MKL1 in MZMs.
MZMs from the indicated mouse spleens FACS sorted as CD11b^{lo}F4/80^{neg}SIGN-R1^{+}I-A^{b-} cells. Cells were cytospun to histology slides and were stained for intracellular expression of MKL1 and were further countered stained with phalloidin for F-actin polymerization (green). Photomicrographs were obtained and the intensity of MKL1 and F-actin was quantitated using the ImageJ program. Representative histograms of the intensity of MKL1 (left panels) or phalloidin (right panels) in sorted MZMs from each indicated mouse group were shown (≥ 20 cells were quantitated per mouse). All data are mean intensity ± SEM (*** P < 0.005 between the indicated groups. n = 2-3 mice per group for 2 independent experiments, Student's t-test).

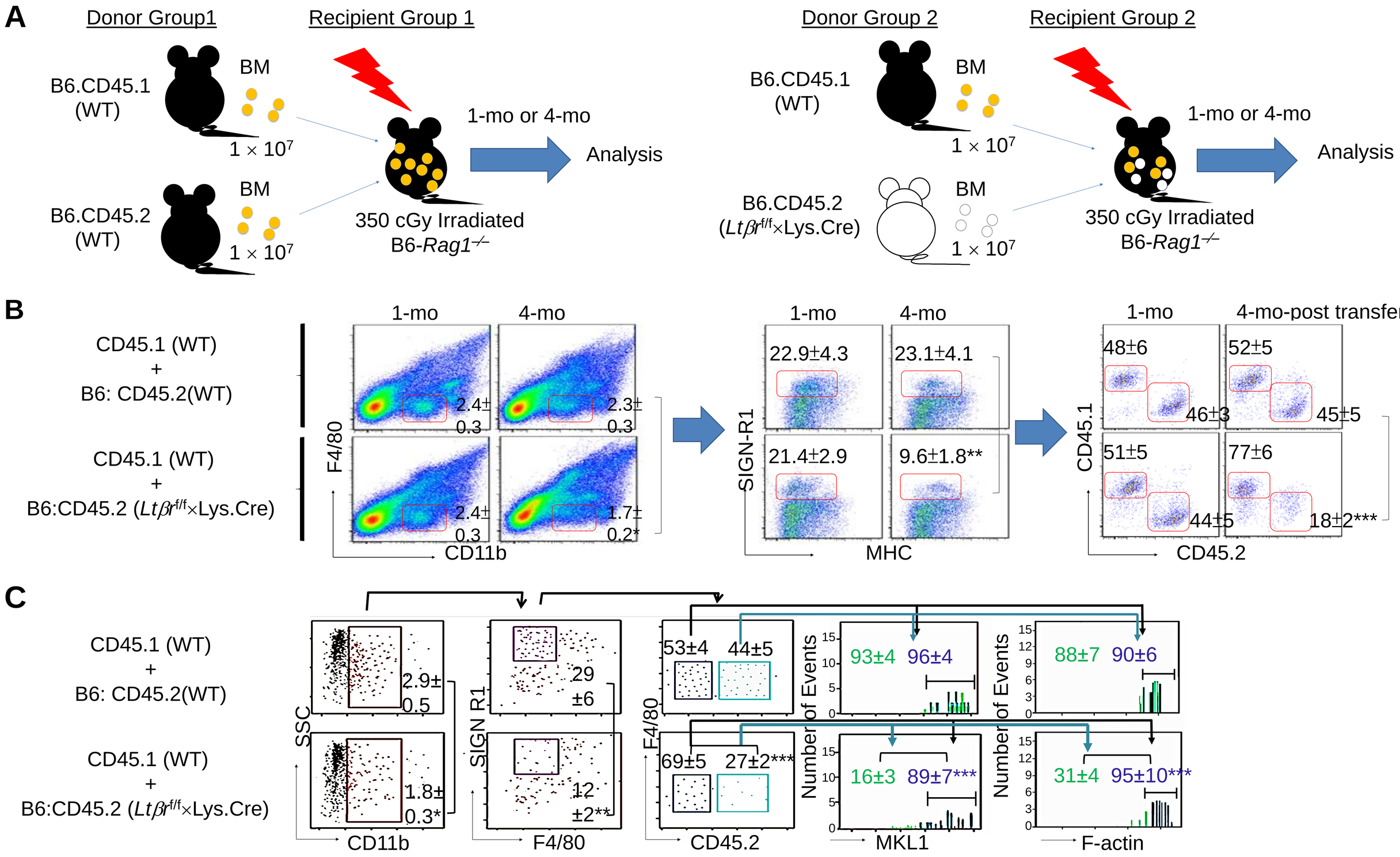

Supplemental Figure 7. Decreased percent of MZMs derived from B6 *Ltβr*$^{f/f}$ ×Lys.Cre mice after mixed BM reconstitution.
(**A**) Mixed BM chimeric mice were generated by reconstitution of equal numbers of Group 1 (CD45.1 B6:CD45.2 B6 BM cells) or Group 2 (CD45.1 B6:CD45.2 B6 *Ltβr*$^{f/f}$ ×Lys.Cre BM cells (10^7 each) into irradiated B6-*Rag1* $^{-/-}$ mice (6-week-old) and analyzed 1 or 4 months later. (**B**) FACS analysis of the percent of MZMs derived from either WT or *Ltβr*$^{f/f}$×Lys.Cre donor BMs. MZMs were gated as CD11b^{lo}F4/80^{neg}SIGN-R1^{+}I-A^{b-} cells and were further gated to show the distribution of CD45.1 or CD45.2 donor cells. (**C**) Sequential ImageStream gating for the expression of MKL1 and F-actin in recipient spleen MZMs 4 months following the transfer of BM cells. Results are mean percent of cells in the gated region ± SEM (*n* = 2-3 per group for 2 independent experiments, **P* < 0.05, ***P* < 0.01, ****P* < 0.005 between results from the indicated groups, Student's t-test).

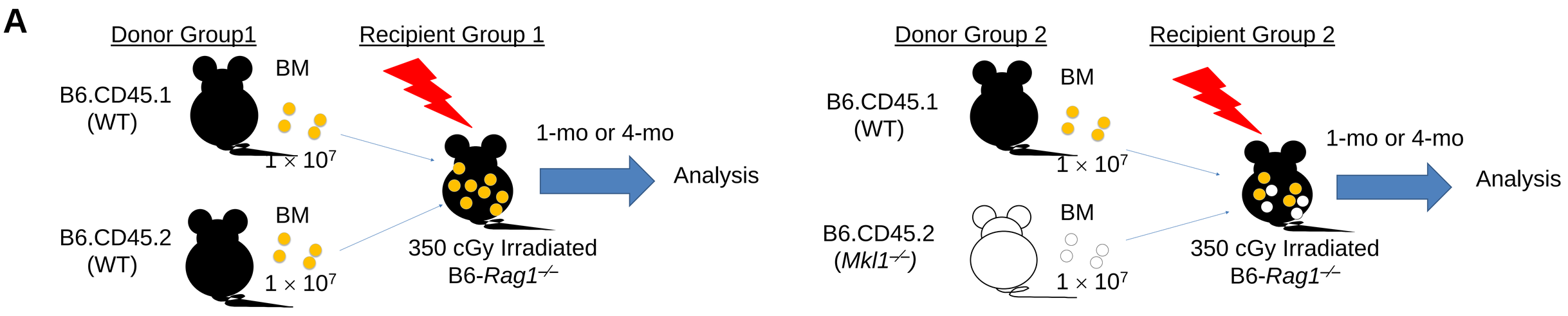

Supplemental Figure 8. Decreased percent and abnormal actin polymerization in MZMs from *Mkl1*$^{-/-}$ mice after mixed BM reconstitution. (**A**) Mixed bone marrow chimeric mice were generated by reconstitution of equal numbers (10^7) of Group 1 (CD45.1 [WT]:CD45.2 [WT] BM cells) or Group 2 (CD45.1 [WT]:CD45.2 [*Mkl1*$^{-/-}$] BM cells into B6-*Rag1*$^{-/-}$ mice (6-weeks-old) and analyzed 1 or 4 months later. (**B**) FACS analysis of the percent of MZMs derived from either WT or *Mkl1*$^{-/-}$ donor BMs. MZMs were gated as CD11b^{lo}F4/80^{neg}SIGN-R1^{+}I-A^{b-} cells and were further gated to show the distribution of CD45.1 or CD45.2 donor cells. (**C**) Sequential ImageStream gating for the expression of MKL1 and F-actin in recipient spleen MZMs 4 months following the transfer of BM derived from WT or *Mkl1*$^{-/-}$ donors. Results are mean percent of cells in the gated region ± SEM (*n* = 2-3 per group for 2 independent experiments, **P* < 0.05, ***P* < 0.01, and ****P* < 0.005 between results from the indicated groups, Student's t-test).

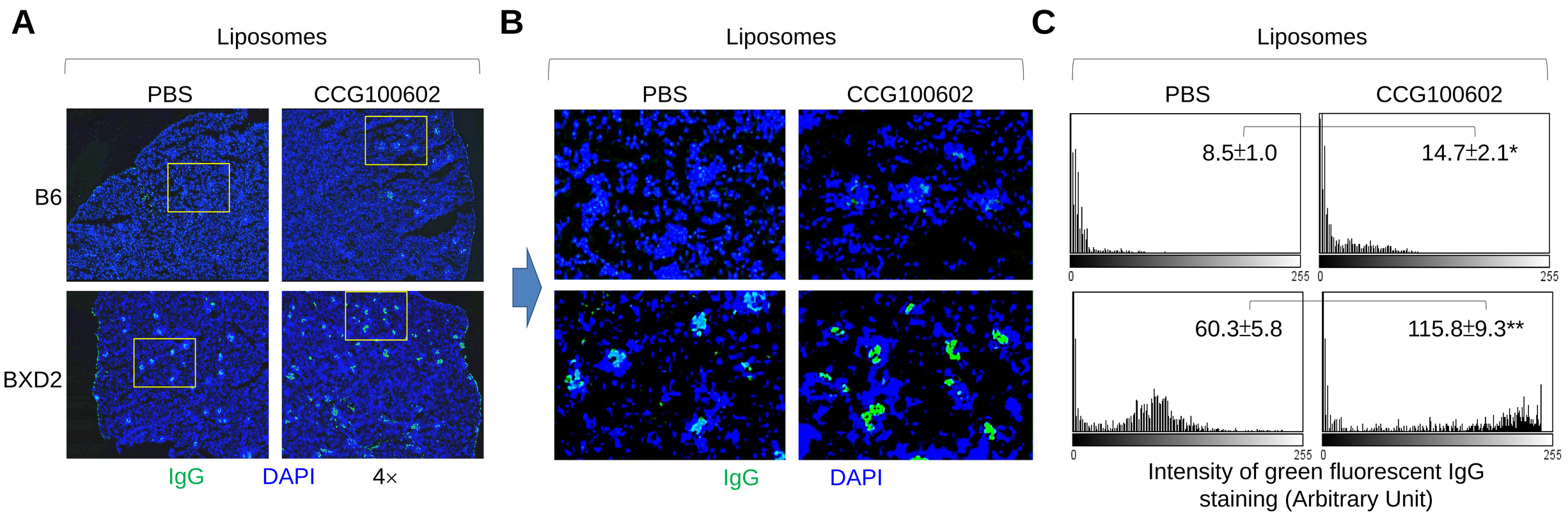

Supplemental Figure 9. Liposome-CCG100602 administration resulted in increased IgG deposition in kidney glomeruli. B6 and BXD2 mice (3-mo-old) were administered i.v. every other day for 4 weeks with liposome-CCG-100602 (100 μg/mouse) or control liposome-PBS. Mice were sacrificed 4 weeks later at 4 months of age. (**A**) Florescence microscopic imaging analysis of IgG^+ glomeruli in the kidney (objective lens, 4×). (**B**) Boxed regions in Panel A are digitally magnified to show a higher power view of the selected region. (**C**) ImageJ analysis of the intensity of IgG in each glomerulus. A representative histogram quantitating the IgG intensity in a representative glomerulus is shown. At least 20 glomeruli were quantitated for each kidney section. Numbers represent mean intensity of green fluorescent ± SEM (*$P < 0.05$ or ** $P < 0.01$ between the indicated comparisons. $n \geq 6$ mice/group, Student's t-test).

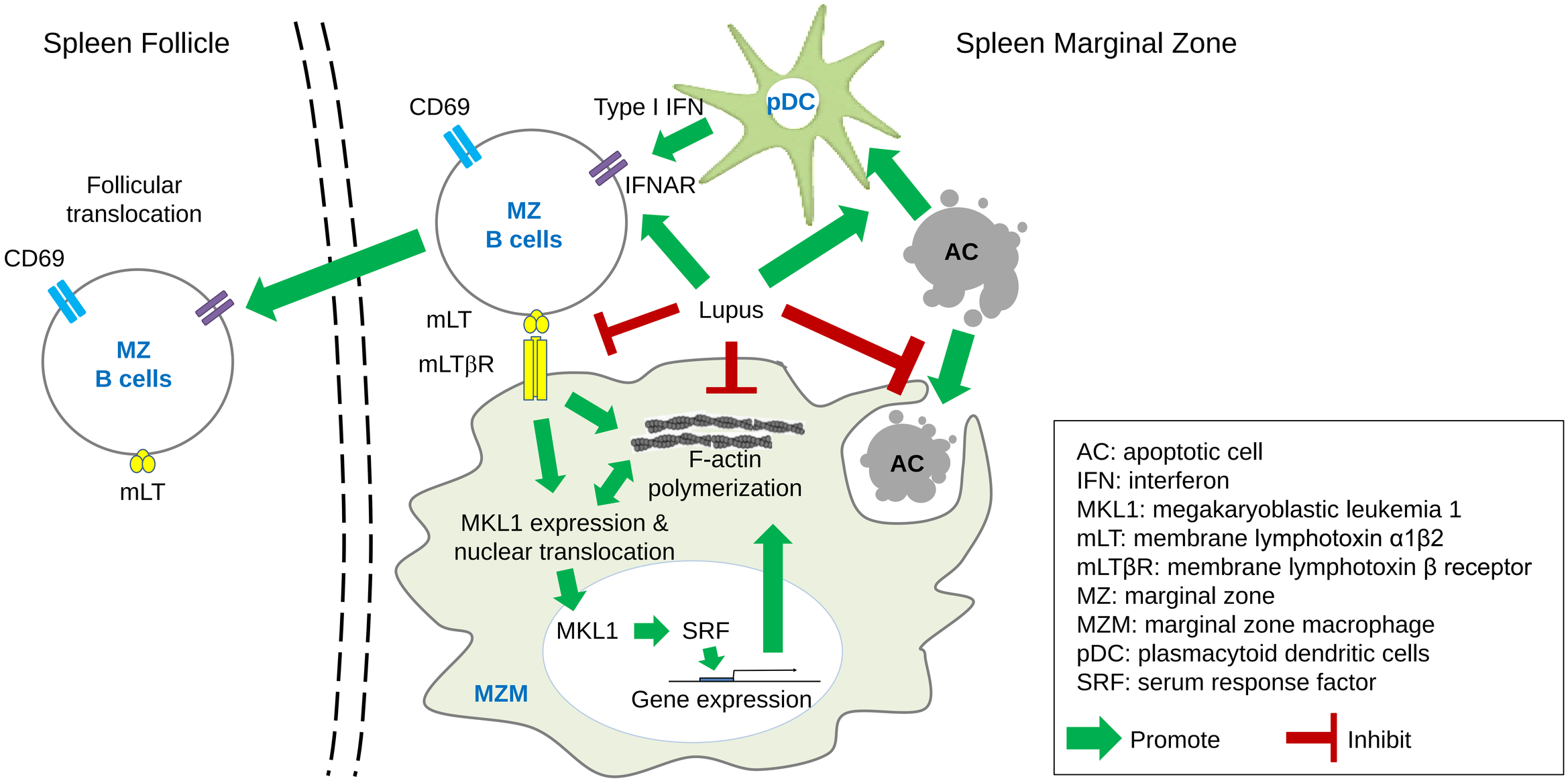

Supplemental Figure 10. Type I IFN disrupts the LTβR/MKL1/F-actin axis leading to defective mechanoreceptor signaling for AC clearance of spleen MZMs.

ACs are normally taken up by scavenger receptors (SR), such as MARCO and SIGN-R1, on MZMs. This process normally leads to tolerogenic signals and decreased AC autoantigens. In lupus, increased interactions of ACs with pDCs in the MZ leads to type I IFN-induced follicular translocation of MZ B cells that disrupts the ability of MZ B cells to signal via mLT through mLTβR on MZMs. Decreased LTβR signaling in MZMs leads to decreased expression and nuclear translocation of MKL1 and defects in SRF. MKL1 is normally localized in the cytoplasm by binding to cytoplasmic G-actin. Mechanical stimulation triggers actin polymerization, liberating MKL1 from G-actin, increasing its nuclear import and accumulation of MKL1, where it co-activates SRF to turn on genes regulating cellular motility and contractility, including vinculin, actin, and SRF. MKL1 and SRF regulate efficient development of endolysosomal vacuoles important for uptake of ACs. In addition, defects in the MKL1/SRF pathway in MZMs leads to altered expression of other genes that can affect function and survival of MZMs. Defects in F-actin polymerization and AC uptake leads to increased ACs and AC debris which further accentuates follicular translocation of MZ B cells. Also, defects in MKL1 and SRF pathways in MZMs lead to first, their loss of AC uptake function and later, decreased MZM survival and loss of MZMs.